ELSEVIER

Journal of Power Sources 68 (1997) 87–90

JOURNAL OF POWER SOURCES

Will advanced lithium-alloy anodes have a chance in lithium-ion batteries?

J.O. Besenhard *, J. Yang, M. Winter

Institute for Chemical Technology of Inorganic Materials, Technical University of Graz, Stremayrgasse 16, 8010 Graz, Austria

Accepted 11 September 1996

Abstract

The high packing density of lithium is a significant advantage of lithium insertion into metallic matrices that can be achieved in lithium alloys compared with lithium intercalation into carbonaceous materials. Moreover, the operating voltage of lithium-alloy anodes may be chosen well-above the potential of metallic lithium and the solvent co-intercalation has not been observed at lithium-alloy electrodes. On the other hand, the volume changes related with insertion/removal of lithium into/from the metallic matrices cause pulverization and rapid failure of lithium-alloy anodes. This paper demonstrates the dramatic effect of the morphology of the metallic host matrix on the performance of the lithium-alloy anodes. Two component host matrices with ultrasmall (submicro- or nanoscale) particle size show an impressive cycling performance. This is related with the small absolute changes of the dimensions of the individual particles and also with the fact that in the first charging step the more reactive particles are allowed to expand in a ductile surrounding of still unreacted material.

Keywords: Lithium-ion batteries; Lithium-alloy anode; Lithium–tin-alloys; Ultrasmall particle size; Multiphase alloys

1. Introduction

Lithium-alloy anodes for rechargeable ambient temperature Li batteries, in particular phase equilibria and transport properties (see Refs. [1,2]), have been thoroughly studied, long before carbonaceous materials were seriously considered for the same application. An obvious advantage of Li insertion into metallic matrices compared with Li intercalation into carbonaceous materials is the high packing density of Li that can be achieved in Li alloys (see Fig. 1(a)). In many cases the packing density of Li (PD_{Li}) is very close to that in metallic Li, or even slightly higher (e.g. $Li_{21}Si_5$: $PD_{Li}=0.0851$ mol/ml, $Li_{21}Sn_5$: $PD_{Li}=0.0724$ mol/ml, $Li_{22}Pb_5$: $PD_{Li}=0.0718$ mol/ml, Li: $PD_{Li}=0.0769$ mol/ml [3]), resulting in impressive volumetric charge densities. As the operating voltage of Li alloys may be chosen well-above the potential of metallic Li (Fig. 2), the problem of Li deposition during charging can be minimized, resulting in improved safety and rapid charging capabilities. Moreover, Li alloys do not seem to suffer from the drawback of solvent co-intercalation.

Unfortunately, the theoretical volume changes related with insertion/removal of Li into/from metallic matrices are quite substantial (usually by a factor of two to three). In the case of alloys characterized by high Li packing density, this results in a fast disintegration (cracking and 'crumbling') of the alloy anodes. On the other side, Li–C anodes are almost dimensionally stable during cycling (see Fig. 1(b)). The topotactic intercalation of Li between the graphene layers of graphitic carbons requires only minor changes of interlayer spacing and stacking order, whereas insertion of Li into metallic matrices causes much more drastic three-dimensional structural rearrangements.

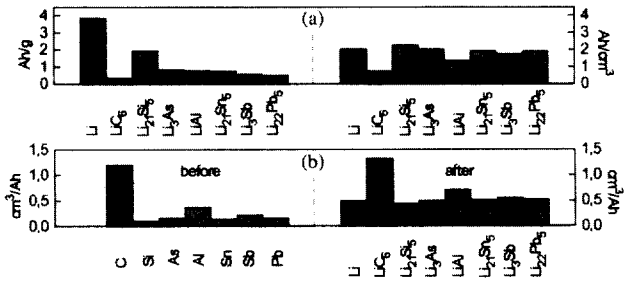

Fig. 1. (a) Gravimetric and volumetric charge densities of anode materials and (b) their volumes (standardized for 1 mole Li storage capacity) before and after Li-insertion [3]. [1]

[1] For Li–Si and Li–Sn alloys slightly different stoichiometries, i.e. $Li_{22}Si_5$ [4] and $Li_{22}Sn_5$ [4,5] have been reported by others.

* Corresponding author.

0378-7753/97/$17.00
PII S0378-7753(96)02547-5

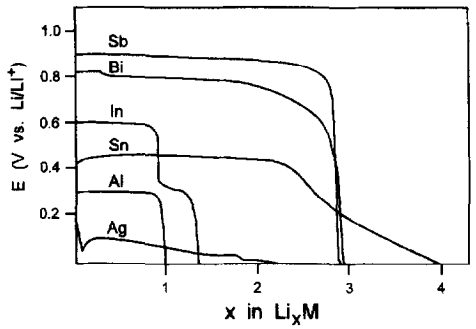

Fig. 2. Charging (=alloying) characteristics of different metals in 1 M $LiClO_4$/PC, $i = 0.025$ mA/cm^2.

The detrimental effect of volume changes of active materials on the performance of battery electrodes during cycling may be compensated for to some extent by proper design of their morphology. In very small particle size active materials even large changes of the dimensions of the crystal structure due to insertion or removal of Li will not necessarily cause cracks and pulverization, as the absolute changes in particle dimensions are still small.

The advantage of very small particle size host materials ('nanomaterials') for Li intercalation has been demonstrated for TiO_2 (anatase) as an anode material for rocking-chair Li batteries [6–8]. Amorphous tin oxide (SnO_x) which can be transformed to metallic Sn during charging, is the anode material of a high energy density rocking-chair battery (theoretical capacity of the anode: 800 mAh/g) recently presented by Fujifilm Celltech [9].

2. Experimental

The metallic host matrices (Sn, Sn–Ag and Sn–Sb) were electroplated onto Cu substrates with constant current densities from aqueous solutions.

1. Pure Sn: (i) small particle sizes of 200–400 nm, see Fig. 5, and (ii) large particle sizes of 2000–4000 nm, see Figs. 3–5, Fig. 9) was plated from (i) 36 g/l $Sn_2P_2O_7$, 135 g/l $K_4P_2O_7$, 0.3 g/l gelatin at 2.5 mA/cm^2, room temperature, stirred solution and (ii) 45 g/l $SnCl_2 \cdot 2H_2O$, 100 g/l $K_4P_2O_7$, 4 g/l tartaric acid, 0.25 g/l gelatin at 2.5 mA/cm^2, at 45 °C, stirred solution.
2. '$Sn_{0.72}Sb_{0.28}$' alloy with particle sizes of 200–400 nm was plated from 30 g/l $SnCl_2 \cdot 2H_2O$, 1.8 g/l $SbCl_3$, 115 g/l $Na_4P_2O_7 \cdot 10H_2O$, 7 g/l tartaric acid, 0.4 g/l gelatin at 2 mA/cm^2, at 44 °C, no stirring.
3. '$Sn_{0.91}Ag_{0.09}$' alloy with particle sizes of 200–400 nm was plated from 55 g/l $Sn_2P_2O_7$, 1.2 g/l AgCN, 220 g/l $K_4P_2O_7$, 8 g/l KCN at 3–4 mA/cm^2, room temperature, no stirring.

Organic electrolyte studies (half-cell studies) were performed in laboratory-type glass cells with excess of electrolyte and battery grade Li-foil counter electrodes. The cycling conditions were as follows: constant current charging (time-controlled), and constant current discharging (potential controlled). Alloy electrodes (on Cu substrate) were not closely packed in separator materials but placed in 1 M $LiClO_4$/PC electrolyte without support or protection. The typical H_2O content of the organic electrolyte was below 20 ppm.

For dilatometric studies a dilatometer with Ni electrodes and a polypropylene body was used, see Ref. [10]. The composition of the alloys was determined by atomic absorption spectroscopy. The interpretation of the X-ray data is based on the JCPDS cards.

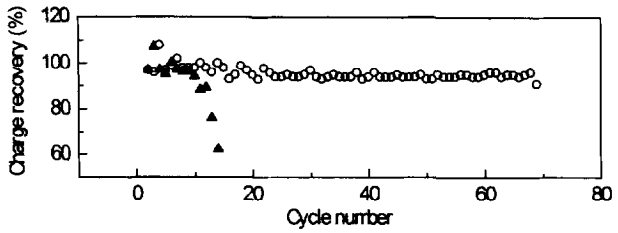

Fig. 3. Cycle life performance of Li_xSn on Cu substrates (wires) of different diameters in 1 M $LiClO_4$/PC, (▲): 1.0 mm, (○): 0.07 mm, thickness of Sn layers: ca. 3 μm, $i_c = i_d = 0.25$ mA/cm^2, charge input: 1.7 Li/Sn; cut-off voltage: 0.9 V vs. Li/Li$^+$.

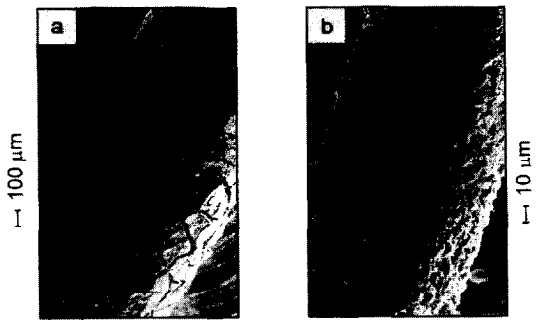

Fig. 4. SEM graphs of Li_xSn anodes in the discharged state, substrate diameters: (a): 1.0 mm, (b): 0.07 mm, cycle No.: 25, charge input: 1.5 Li/Sn (other conditions see Fig. 3).

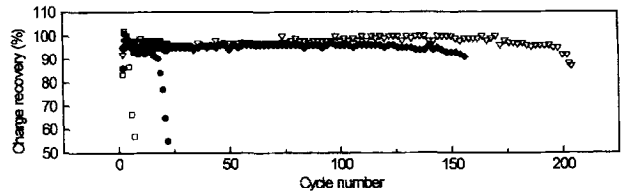

Fig. 5. Cycle life performance of electroplated Sn, $SnSb_n$ and $SnAg_n$ (thickness: ca. 3 μm) on Cu substrates in 1 M $LiClO_4$/PC, $i_c = i_d = 0.25$ mA/cm^2, charge input: 1.7 Li/M, cut-off: 1.2 V vs. Li/Li$^+$, cycling was stopped when input of 1.7 Li/M caused potential to approach 0.0 V vs. Li/Li$^+$, metallic host matrix and its typical particle size: (□): Sn, 2.000–4.000 nm, (●): Sn, 200–400 nm, (◆): Sn + $SnAg_3$/$SnAg_4$ (analytical composition '$Sn_{0.91}Ag_{0.09}$'), 200–400 nm, (▽): Sn + SnSb (analytical composition '$Sn_{0.72}Sb_{0.28}$'), 200–400 nm.

3. Results and discussion

3.1. Cycling performance and morphology of Li-alloy anodes

As a consequence of the volume changes during cycling, good cycling results of Li-alloy anodes have only been

observed if the thickness of the reaction layer was kept in the order of a few μm [11]. The fact that the failing mechanism of Li-alloy anodes is mostly related with cracking and crumbling renders possible a significant improvement of these anodes by relatively simple morphological measures. This is illustrated by Figs. 3 and 4, showing the cycling performance and topography of Li_xSn anodes prepared by electrodeposition of Sn on Cu substrates of different sizes. It can be clearly seen that cracking of Li_xSn can be avoided by reducing the diameter of the wire substrate.

Strong particle size effects have also been observed with electroplated Sn anodes on flat Cu substrates, when the morphology of Sn was changed by the plating conditions. The best results were obtained with fine-grained Sn (typical size 200–400 nm) whereas coarse-grained Sn (typical size 2000–4000 nm) and also highly compact 'specular' Sn behaved very poorly [12].

3.2. *Small particle size multiphase Li-alloy anodes*

Electroplating from solutions containing salts of different plateable metals ('plating of alloys') is a convenient method to create small particle size intermetallic phases, as well as small particles of pure metals or mixtures thereof. The morphology of the plated materials can be drastically changed by variation of the plating conditions. Multiphase Li-insertion anodes consisting of fine-grained and slightly porous deposits of either Sn and SnSb or Sn and $SnAg_n$ (typical grain size: 200–400 nm) have been prepared in this way [12]. Their

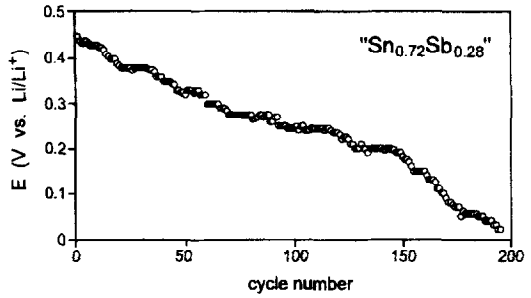

Fig. 6. Drift of the end of charge potential for cycling of $SnSb_n$ in 1 M $LiClO_4$/PC, cycling conditions see Fig. 5.

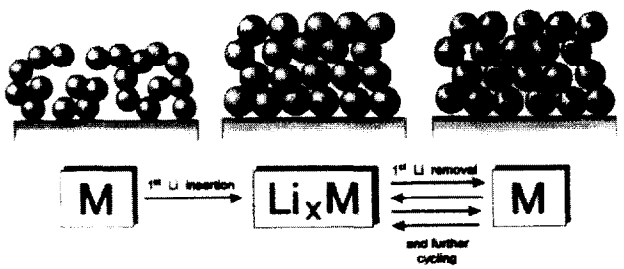

Fig. 7. Model of lithium insertion into a loosely packed small particle size metallic matrix. Even 100% volume expansion of individual particles does not crack them as their absolute changes in dimensions are still small. Removal of lithium from the Li_xM particles does not necessarily affect very much the size of the expanded particles, i.e. the overall dimensions of the electrode remain almost constant in the further cycles.

cycling performance is by far better than that of pure Sn deposits of comparable grain size (see Fig. 5).

Cycle numbers up to 700 have been achieved with $LiCoO_2$ as the cathode material when the charge input was limited to 1.2 Li/M.

The constant capacity charging in combination with potential-controlled discharging causes a drift of the end of charge potential as any losses of active material M increase the ratio Li/M (Fig. 6).

Judging from scanning electron microscopy (SEM) graphs, the drastic differences in cycling performance are paralleled by the extent of pulverization. Whereas pure Sn is severely cracked and finally delaminated, the morphology of the $SnSb_n$ and $SnAg_n$ matrix, respectively, remains fairly intact even after a larger number of cycles. SEM graphs of $SnSb_n$ and $SnAg_n$ electrodes taken after a few cycles only look similar as those SEM graphs taken after about 150 cycles (for cycling conditions, see Fig. 5). This behaviour suggests that drastic morphological changes occur only during the first cycle, whereas in the long run the electrode is approaching a more 'dimensionally stable' situation, see Fig. 7.

X-ray studies [13] as well as the potential–composition diagram of the first insertion of Li into the Sn/SnSb phase mixture clearly show that the SnSb phase is reacting first, i.e. has the chance to expand embedded in a soft and ductile Sn matrix, see Fig. 8. The potential of Li insertion into SnSb is very close to that of Li insertion into Sb (see Fig. 2), the multistep formation of phases Li_xSn is in good agreement with data published previously by Huggins and co-workers [1,14]. The length of the first plateau in Fig. 8 corresponds to the formation of Li_3Sb. This result was confirmed by varying the ratio of the Sn/Sn–Sb host matrices.

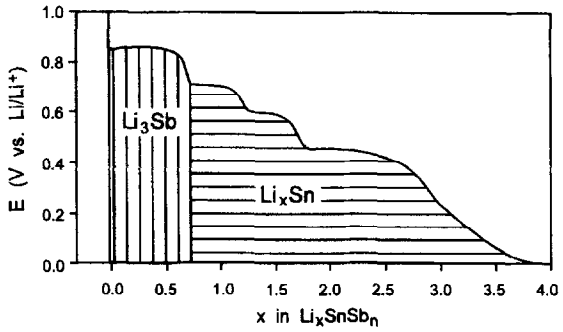

Fig. 8. Potential/composition diagram of a '$Sn_{0.72}Sb_{0.28}$' electrode consisting of Sn and SnSb in 1 M $LiClO_4$/PC, $i = 0.025$ mA/cm^2.

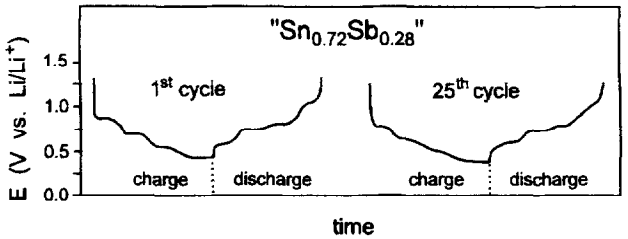

Fig. 9. Charge/discharge diagram of a '$Sn_{0.72}Sb_{0.28}$' electrode in 1 M $LiClO_4$/PC, $i_c = i_d = 0.25$ mA/cm^2, charge input: 1.7 Li/M.

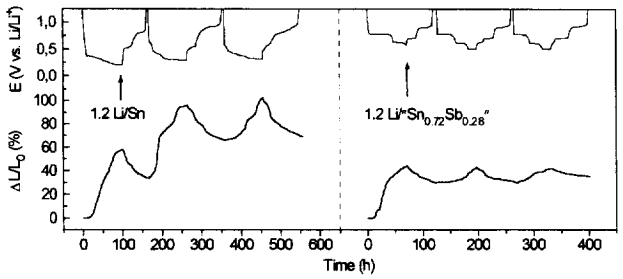

Fig. 10. Recordings of potential and relative thickness of Sn and $SnSb_n$ on a Cu substrate during cycling in 1 M $LiClO_4$/PC, charge input: 1.2 Li/M, cut-off: 2 V vs. Li/Li^+, typical particle size: 2.000–4.000 nm for Sn, 200–400 nm for Sn + SnSb (analytical composition '$Sn_{0.72}Sb_{0.28}$').

Charge/discharge diagram (see Fig. 9) and X-ray data of '$Sn_{0.72}Sb_{0.28}$' electrodes do not change very much between the first and the following several cycles, indicating that SnSb may be reconstructed during discharge. On the other hand, the X-ray information is getting poorer with increasing cycle number due to structural disintegration of the host matrices [12].

Dilatometric in situ studies of the expansion/contraction of Li-alloy electrodes during cycling are in some agreement with the model presented in Fig. 7. Dimensional changes of $SnSb_n$ electrodes during cycling turned out to be quite small after the first insertion of lithium. By contrast, the 'breathing' of pure Sn was much more drastic (Fig. 10).

4. Conclusions

Dimensional changes and 'pulverization' failure of Li-alloy electrodes during cycling can be minimized in small particle size multiphase alloy matrices.

Acknowledgements

One of us (J.Y.) is obliged to the Academic Exchange Service of Germany for a grant. Parts of this work were supported by FWF, Austria, in the 'Electroactive Materials' special research program.

References

[1] J. Wang, I.D. Raistrick and R.A. Huggins, *J. Electrochem. Soc., 133* (1986) 457.
[2] J.O. Besenhard, in W. Müller-Warmuth and R. Schöllhorn (eds.), *Progress in Intercalation Research*, Kluwer, Dordrecht, 1994, p. 457.
[3] R. Nesper, *Prog. Solid State Chem., 20* (1990) 1.
[4] R.A. Huggins, in B. Scrosati, A. Magistris, C.M. Mari and G. Mariotto (eds.), *Fast Ion Transport Solids*, Kluwer, Dordrecht 1993, p. 143.
[5] F.A. Shunk, *Constitution of Binary Alloys, Second Supplement*, McGraw Hill, New York, 1969, p. 481.
[6] M. Grätzel, *Chem. Tech., 67* (1995) 1300.
[7] S.Y. Huang, L. Kavan, I. Exnar and M. Grätzel, *J. Electrochem. Soc., 142* (1995) L142.
[8] L. Kavan, M. Grätzel, J. Rathousky and A. Zukal, *J. Electrochem. Soc., 142* (1995) 394.
[9] Y. Idota, Fujifilm Celltech Co. Ltd. personal communication.
[10] W. Biberacher, A. Lerf, J.O. Besenhard, H. Möhwald and T. Butz, *Mater. Res. Bull., 17* (1982) 1385.
[11] M. Garreau, J. Thevenin and M. Fekir, *J. Power Sources, 9* (1983) 235.
[12] J. Yang, M. Winter and J.O. Besenhard, *Solid State Ionics, 90* (1996) 281.
[13] J. Yang, *Ph.D. Thesis*, University of Münster, Germany, 1995.
[14] R.A. Huggins, *J. Power Sources, 26* (1989) 109.